

# Halo Velocity Groups in the Pisces Overdensity

Branimir Sesar<sup>1</sup>, A. Katherina Vivas<sup>2</sup>, Sonia Duffau<sup>3</sup>, Željko Ivezić<sup>1</sup>

## ABSTRACT

We report spectroscopic observations with the Gemini South Telescope of 5 faint ( $V \sim 20$ ) RR Lyrae stars associated with the Pisces overdensity. At a heliocentric and galactocentric distance of  $\sim 80$  kpc, this is the most distant substructure in the Galactic halo known to date. We combined our observations with literature data and confirmed that the substructure is composed of two different kinematic groups. The main group contains 8 stars and has  $\langle V_{gsr} \rangle = 50$  km s<sup>-1</sup>, while the second group contains four stars at a velocity of  $\langle V_{gsr} \rangle = -52$  km s<sup>-1</sup>, where  $V_{gsr}$  is the radial velocity in the galactocentric standard of rest. The metallicity distribution of RR Lyrae stars in the Pisces overdensity is centered on  $[Fe/H] = -1.5$  dex and has a width of 0.3 dex. The new data allowed us to establish that both groups are spatially extended making it very unlikely that they are bound systems, and are more likely to be debris of a tidally disrupted galaxy or galaxies. Due to small sky coverage, it is still unclear whether these groups have the same or different progenitors.

*Subject headings:* stars: variables: other — Galaxy: halo — Galaxy: kinematics — Galaxy: structure

## 1. Introduction

In the last decade, abundant observational evidence has been accumulated in favor of a hierarchical formation scenario of the halo of the Milky Way (see a review by Helmi 2008). The substructures in the halo have been observed both as overdensities in space and as moving groups. The tidal streams of the disrupting Sagittarius dwarf spheroidal (dSph) galaxy

---

<sup>1</sup>University of Washington, Department of Astronomy, P.O. Box 351580, Seattle, WA 98195-1580; {bsesar, zi}@u.washington.edu

<sup>2</sup>Centro de Investigaciones de Astronomía (CIDA), Apartado Postal 264, Mérida 5101-A, Venezuela; akvivas@cida.ve

<sup>3</sup>Astronomisches Rechen-Institut, Zentrum für Astronomie der Universität Heidelberg, Mönchhofstraße 12-14, D-69120 Heidelberg, Germany; sonia.duffau@gmail.com

are the best example of such substructures, with the streams wrapping around most of the sky (Ivezić et al. 2000; Yanny et al. 2000; Vivas et al. 2001; Ibata et al. 2002; Majewski et al. 2003). Other known substructures include the Virgo Stellar Stream (Duffau et al. 2006; Prior et al. 2009) and several other small structures associated with the Virgo overdensity (Newberg et al. 2007; Jurić et al. 2008; Vivas et al. 2008), the Monoceros structure (Ibata et al. 2003; Yanny et al. 2003; Ivezić et al. 2008a), the Triangulum-Andromeda overdensity (Rocha-Pinto et al. 2004), the Hercules-Aquila cloud (Belokurov et al. 2007a), the Orphan stream (Belokurov et al. 2007b), and other smaller overdensities (Clewley & Kinman 2006; Starkenburg et al. 2009) and streams (Grillmair 2009; Schlafman et al. 2009). Using Sloan Digital Sky Survey (SDSS; York et al. 2000) multi-epoch data in the stripe 82 region ( $308^\circ < R.A. < 60^\circ$ ,  $|Dec| < 1.25^\circ$ ), Sesar et al. (2007) found an overdensity of RR Lyrae stars in the halo at a heliocentric and galactocentric distance of  $\sim 80$  kpc and  $R.A. \sim 354^\circ$  (termed “Structure J”, see Figures 10 and 11 from Sesar et al. 2010). This structure was subsequently renamed the “Pisces overdensity” by Watkins et al. (2009) after the constellation where it is located.

Convincing evidence that the Pisces overdensity is indeed a coherent structure, and not a random superposition of stars, was recently presented by Kollmeier et al. (2009). They measured radial velocities of 8 RR Lyrae stars located in the Pisces overdensity and found that 5 of them have a narrow velocity distribution centered on  $\sim -75$  km s $^{-1}$  in the heliocentric rest frame. The authors found hints of a second velocity peak in their data, containing two or maybe three stars, at a lower velocity ( $< -150$  km s $^{-1}$  in the heliocentric rest frame). Kollmeier et al. (2009) interpreted the main peak as a dwarf galaxy or a disrupting dwarf galaxy, and did not consider the second peak as a real group due to a small number of stars. In this paper, we expand on their work by reporting radial velocities and metallicities for 5 RR Lyrae stars in the Pisces overdensity, four of which were not observed by Kollmeier et al. (2009). By combining these two data sets, we are now in position to confirm the existence of a second peak in the velocity distribution, and are able to better explore the spatial extent and metallicity distributions of these two substructures present in the Pisces overdensity.

## 2. Observations

### 2.1. Target Selection

In Figure 1 we show the spatial distribution of *ab*-type RR Lyrae (RRab) stars in the Pisces region. The stars were selected from the publicly available Sesar et al. (2010) catalog. Kollmeier et al. (2009) obtained spectra of 8 of these stars located in the densest part of this region (solid circles and one starred symbol in Figure 1). Our targets (starred symbols)

for spectroscopic observations were mainly chosen to expand the coverage in direction of equatorial right ascension. As seen in Figure 1, with the addition of our targets all RR Lyrae stars in the densest part of the overdensity now have spectroscopic measurements.

The positions, periods, and epochs of maximum brightness ( $HJD_0$ ) of RR Lyrae stars observed in this work are listed in Table 1 and their  $g$ -band light curves are shown in Figure 2. The periods and epochs of maximum brightness are precise to within a few seconds and minutes, respectively, allowing the phase of pulsation to be determined with a 1% uncertainty (Sesar et al. 2010). The precise estimate of phase is important when subtracting the velocity due to pulsations from the measured radial velocity, as we explain in Section 2.2. Star 343892 (indicated by an arrow in Figure 1) is in common with Kollmeier et al.’s sample and provides a good check on the consistency of both works.

The heliocentric distances of RR Lyrae stars,  $d$ , are estimated from measurements of their flux-averaged and dereddened  $V$ -band magnitudes,  $\langle V \rangle$  (for details see Sesar et al. 2010), and by assuming an average value for their absolute magnitudes of  $M_V = 0.6$ . This value was obtained by using the Chaboyer (1999)  $M_V - [Fe/H]$  relation

$$M_V = (0.23 \pm 0.04)[Fe/H] + (0.93 \pm 0.12) \quad (1)$$

and adopting  $[Fe/H] = -1.5$  as the metallicity of RRab stars (the median halo metallicity, see Ivezić et al. 2008a). This metallicity is used when calculating distances even though for some stars we measure spectroscopic metallicities later in the paper. The fractional error in the heliocentric distance due to halo metallicity dispersion ( $\sigma_{[Fe/H]} = 0.3$  dex, Ivezić et al. 2008a) and RR Lyrae evolution off the zero-age horizontal branch, is estimated at 6% ( $\sim 5$  kpc error in distance at 80 kpc). Due to their angular position, the heliocentric and galactocentric distances of these stars are virtually the same. The apparent  $\langle V \rangle$  magnitudes of the observed stars range from 20.05 mag to 20.21 mag, corresponding to distances of 78 kpc and 84 kpc, respectively. The spread in distances is consistent with the uncertainty in distance.

## 2.2. Spectroscopic Observations

The spectroscopic observations were obtained during 2009 Aug 19-21 using the Gemini Multi-object Spectrograph (GMOS; Allington-Smith et al. 2002) mounted on the 8.1-m Gemini South telescope at Cerro Pachon, Chile. Bad weather on two of the three nights did not allow us to observe more than 5 targets. A  $1''$  long-slit was used with the B1200 grating, resulting in a resolution of  $R = 1820$ , or  $\sim 2.5 \text{ \AA}$  at  $4500 \text{ \AA}$ . This is equivalent to a resolution of  $\sim 150 \text{ km s}^{-1}$  at  $H\beta$ . The spectral range extends from  $3800 \text{ \AA}$  to  $5250 \text{ \AA}$ . The Pisces

overdensity targets were observed in two sets of 2700s-exposures centered on  $\lambda_{\text{central}} = 4500 \text{ \AA}$  and  $\lambda_{\text{central}} = 4550 \text{ \AA}$  (to account for the gaps in the detector), with each exposure set bracketed by observations of a CuAr arc lamp. The difference in resolution between the two setups (different  $\lambda_{\text{central}}$ ) is very small ( $2.45 \text{ \AA}$  vs  $2.47 \text{ \AA}$ ). Nevertheless, each set of spectra was reduced and calibrated independently, and only then they were combined. The total exposure time (1.5 hours) is  $\lesssim 12\%$  of the pulsation cycle of these RR Lyrae stars. Therefore, we do not expect excessive broadening of spectral features due to the changing radial velocity during the pulsation cycle (broadening  $\lesssim 13 \text{ km s}^{-1}$ ).

Images were processed using the *gmos* package in IRAF. Cosmic rays were removed using the L.A. Cosmic routine<sup>1</sup> (van Dokum 2001). Wavelength calibration was done using  $\sim 40$  CuAr arc spectral features over the whole spectrum. The median root-mean-square (rms) scatter of the fit of the wavelength calibration was  $0.03 \text{ \AA}$ , or  $2 \text{ km s}^{-1}$ . The signal-to-noise ratio (S/N) of the final spectra ranged from 20 to 30 at  $\sim 4000 \text{ \AA}$ . Figure 3 shows the spectra of the 5 targets, ordered from the lowest to highest S/N. Balmer lines (starting at  $H\beta$ ) and Ca II H and K lines are easily seen in the spectra.

We observed stars between phases 0.2 and 0.7 of the pulsation cycle in order to avoid the discontinuity in the radial velocity curve near the maximum light. As expected, the best S/N was achieved for stars observed during the descending part of the light curve (phases 0.2 to 0.5) rather than during minimum light (phase  $> 0.5$ , e.g. star 490555). Radial velocities,  $V_r$ , were obtained by cross-correlating our spectra with 13 standard star spectra taken from the ELODIE catalog<sup>2</sup> (Moultaka et al. 2004), which were degraded to the resolution of our observations (convolved with the instrumental line profile and repixelized). For the instrumental line profile, we use the line profile measured around the central part of the spectrum (i.e., the line profile is assumed to be independent of wavelength). The velocity measurements are not significantly affected by this assumption, as measured velocities of three HD radial velocity standard stars indicate below. The ELODIE radial velocity standard stars have spectral types between F2 and F9. The systemic (center-of-mass) velocity of RR Lyrae stars,  $V_\gamma$ , was obtained following the procedure described in detail in Vivas et al. (2005, 2008). Here, we only summarize the most important points. We used the radial velocity curve of RRab star X Arietis as a template. The template was shifted in velocity to match the measurement for each star at the corresponding phase and the systemic velocity is that of the shifted template at phase 0.5.

Table 2 shows different errors that contribute to the final (systemic) velocity error. First,

---

<sup>1</sup>available at [HREF]<http://www.astro.yale.edu/dokkum/lacosmic/>

<sup>2</sup>[HREF]<http://atlas.obs-hp.fr/elodie/>

there is the cross-correlation error reported by *fxcor*. This error includes the uncertainties due to broadening of spectral features during an exposure, random errors in wavelength calibration, and errors due to ELODIE template mismatch. The  $\sigma_{cc}$  value listed in Table 2 is the average cross-correlation error value obtained from 13 cross-correlations. The radial velocity ( $V_r$ ) listed in Table 1 is the mean of 13  $V_r$  values obtained from cross-correlations, where each  $V_r$  value is weighted by its cross-correlation error. Therefore, radial velocities from better template fits contribute more towards the final radial velocity value. The consistency of radial velocity measurement obtained from cross-correlations is good ( $\sim 3 \text{ km s}^{-1}$ ), as indicated by the standard deviation  $\sigma_{\text{templates}}$ .

The cross-correlation error may not fully represent the true error in the radial velocity since it does not include systematic errors in the wavelength calibration. To assess this issue, we cross-correlated 7 spectra of three radial velocity standards (HD 154417, HD 155967 and HD 180482) which were observed during our observing run with the same instrumental setup, with ELODIE standards. The velocities of standards were recovered with a mean difference of  $-1.7 \text{ km s}^{-1}$  from literature values; the standard deviation of the differences is only  $3 \text{ km s}^{-1}$ . The maximum difference is  $6 \text{ km s}^{-1}$ , which we assume as the maximum error in the wavelength calibration. The error in the radial velocity ( $\sigma_r$ ) was obtained by adding this value in quadrature with the cross-correlation error. The average error of our radial velocity measurements is  $11 \text{ km s}^{-1}$ . Finally, the error calculation for the systemic velocity includes terms that take into account errors in the model radial velocity curve. Following Vivas et al. (2005), we use the following expresion in which the second term accounts for likely uncertainties in the phase where the velocity curve passes through the systemic velocity, and the third term is related to possible variations in the slope of the velocity curve:

$$\sigma_\gamma^2 = \sigma_r^2 + (119.5 * 0.1)^2 + (23.9 * \Delta\phi)^2 \quad (2)$$

where  $\Delta\phi = \phi_{obs} - 0.5$ , and  $\phi_{obs}$  is the phase of observation. The contributions of model uncertainties,  $\sigma_{\text{model}}$ , to final velocities are indicated in Table 2 ( $\sigma_{\text{model}}^2 = (119.5 * 0.1)^2 + (23.9 * \Delta\phi)^2$ ). These are of the same order as the observed radial velocity errors. Therefore, to reduce the uncertainty in the systemic velocity we need to reduce the uncertainty introduced by the model, that is, we need to observe the radial velocity curve more than once. The final errors in systemic velocities,  $\sigma_\gamma$ , range from 10 to  $18 \text{ km s}^{-1}$ .

In the case of star 343892 we fitted the template to both our measurement and the one reported by Kollmeier et al. (2009). The fit is shown in Figure 4. The radial velocity curve of X Arietis fits well to both observations. This good agreement gives us confidence that there are no large systematic differences between our measurements and those reported by Kollmeier et al. (2009). The systemic velocity of this star reported in Table 1 corresponds to the one obtained by the fit of the template and differs somewhat from the value assumed

by Kollmeier et al. (see Section 2.3). In this case, the final error was calculated as  $(\sigma_{\gamma, Koll}^{-2} + \sigma_{\gamma, This\ work}^{-2})^{-1/2}$  (standard deviation of a weighted mean).

Finally, we calculated the velocity seen by an observer at the Sun who is at rest with the Galactic center,  $V_{gsr}$ , by assuming solar motion of  $(v_U, v_V, v_W) = (10.0, 5.2, 7.2)$  km s<sup>-1</sup> and  $v_{LSR} = 220$  km s<sup>-1</sup> (Binney & Merrifield 1998).

The spectroscopic metallicities were measured following the method and calibration of Layden (1994) which involves plotting the pseudo-equivalent width of Ca II K line,  $W(K)$ , corrected for interstellar Ca absorption, against the mean pseudo-equivalent widths of  $\beta$ ,  $\gamma$ , and  $\delta$  Balmer lines,  $W(H)$  (see Vivas et al. 2005, 2008, for details). With this method, we estimated metallicity errors of 0.15 dex. Due to low S/N, the metallicity for star 377927 has higher uncertainty (0.2 dex), and for star 490555 the metallicity was not measured at all (see Table 1).

### 2.3. Data from Kollmeier et al. (2009)

As shown in Figure 4, there is a consistency between our radial velocities and the ones measured by Kollmeier et al. (2009). However, the methods that were used to obtain the systemic velocity differ between the two works. In order to avoid differences when combining samples, we decided to take their reported radial velocities (uncorrected for pulsations) and use our method (that is, fitting the template of X Arietis) to uniformly derive systemic velocities. When our method is applied to their measurements, we find a systematic difference of  $\sim 15$  km s<sup>-1</sup> (our values are larger than Kollmeier et al.’s). Our main conclusions are not affected by this difference. For reference, the original and revised Kollmeier et al. (2009) velocities are listed in Table 3. In the following section we use only the revised systemic velocities.

Kollmeier et al. also provide spectroscopic metallicities calibrated using the Gratton et al. (2004) method. For star 343892 that is common to both samples, we measure the metallicity of -1.1 dex while Kollmeier et al. measured -1.2 dex. It is quite encouraging that the two metallicity estimates are consistent within uncertainties, considering different instruments and calibration methods. Given this consistency, we simply combine our and Kollmeier et al.’s metallicities when presenting results in the next section.

## 3. Results and Discussion

In this Section we address the following questions:

1. What is the mean velocity and velocity dispersion of our sample, and how do these values compare to the literature?
2. Is the observed distribution of velocities a Gaussian or a non-Gaussian distribution?
3. Are the observed velocity groups bound or unbound systems?
4. What does the metallicity of stars say about the progenitor(s) of the streams?

Figure 5 shows the distribution of velocities of 12 RRab stars in the Pisces overdensity from the combined data set. The weighted mean velocity, velocity dispersion, and their uncertainties for the full sample are  $\langle V_{gsr} \rangle = 7 \pm 16 \text{ km s}^{-1}$  and  $\sigma_{gsr} = 56 \pm 12 \text{ km s}^{-1}$ . If the sample is divided into positive (8 stars) and negative velocities (4 stars), the values are  $\langle V_{gsr}^{pos} \rangle = 50 \pm 3 \text{ km s}^{-1}$ ,  $\sigma_{gsr}^{pos} = 10 \pm 3 \text{ km s}^{-1}$ ,  $\langle V_{gsr}^{neg} \rangle = -52 \pm 11 \text{ km s}^{-1}$ , and  $\sigma_{gsr}^{neg} = 23 \pm 9 \text{ km s}^{-1}$ .

The measured velocity dispersion for the full sample is consistent with the halo velocity dispersion profile obtained by Brown et al. (2010) using a sample of 910 distant halo stars. By extrapolating their Equation 6 to 83 kpc, we obtain a velocity dispersion of  $73 \text{ km s}^{-1}$ ; a slightly higher dispersion than the one we measure, but still within  $\sim 1\sigma$  uncertainties. Since the (Brown et al. 2010) sample covers a greater area of the sky than our sample ( $7300 \text{ deg}^2$  vs.  $23 \text{ deg}^2$ ), it is also more likely to contain a greater number of velocity groups at large distances than our sample. If these groups have different internal kinematics (mean velocities and velocity dispersion), the net effect will be a higher velocity dispersion in the sample with more velocity groups. We have also searched the Brown et al. (2010) catalog for blue horizontal branch stars that might be associated with the Pisces overdensity and found one possible candidate. This star has R.A. =  $355.575542 \text{ deg}$ , Dec =  $0.326697 \text{ deg}$ ,  $V_{gsr} = 101 \pm 17 \text{ km s}^{-1}$ , and is at a distance of 74 kpc. The uncertainty in distance is  $\sim 6\%$ , same as for RR Lyrae stars. However, we do not think this star is related to the Pisces overdensity as its velocity is at least  $3\sigma$  away from the positive velocity peak at  $\langle V_{gsr}^{pos} \rangle = 50 \text{ km s}^{-1}$ , where  $\sigma = \sigma_{gsr}^{pos} = 10 \pm 3 \text{ km s}^{-1}$ .

The question of whether the distribution of velocities shown in Figure 5 is a Gaussian or non-Gaussian distribution is an important one, as deviations from normality are usually interpreted as a signature of velocity groups in the smooth halo component (Harding et al. 2001; Duffau et al. 2006; Vivas et al. 2008). To test for the presence of velocity groups in the halo, Harding et al. (2001) recommend the Shapiro & Wilk (1965) (SW) statistical test of normality to be applied to velocity histograms. This test is sensitive to many different deviations from the Gaussian shape and does not depend on the choice of mean or dispersion of the normal distribution (see Harding et al. 2001 Section 5.1 and D’Agostino & Stephens 1986 for more details on the test).

The null hypothesis of the SW test is that a sample came from a normally distributed population. To test a sample, we use the *shapiro.test* routine provided by the *R* statistical package<sup>3</sup>. This routine evaluates the *W* test statistic for a sample, and estimates its *P*-value for any *n* in the range  $3 \leq n \leq 5000$ , where *n* is the sample size. For example, if the *P*-value of a tested sample is less than 0.05, it can be concluded that the data are not drawn from a normally distributed population at the 95% confidence level.

The *P*-value is the probability of obtaining a test statistic at least as extreme as the one that was actually observed, assuming that the null hypothesis is true. If we know that the null hypothesis is true, e.g. we generate samples by drawing values from a Gaussian distribution, the test is reliable if the fraction of samples with  $P < \alpha$  does not exceed  $\alpha$ . We use Monte Carlo simulations to estimate the reliability of the *P*-value provided by the SW test for small samples. We generate 10,000 samples and for each sample draw 12 values from a Gaussian distribution. Assuming a fiducial value of  $\alpha = 0.01$ , we find that less than 1% of samples have *P*-values less than 0.01. A similar result is obtained for  $\alpha = 0.05$ . These results show that the *P*-value provided by the SW test is reliable even when testing small samples: the false rejection rate is less than the adopted value of  $\alpha$ .

The SW test accepts single-valued data points and does not take into account uncertainties in measurements. To account for uncertainties in measured velocities when applying the SW test, we use Monte Carlo simulations. We generate 10,000 samples and for each sample draw 12 velocities from 12 Gaussian error distribution (one velocity per Gaussian). These Gaussians are centered on measured velocities and have widths equal to uncertainties in measured velocities. We then obtain a *P*-value for each sample using the SW test. The most likely (mode) *P*-value for these samples is  $\sim 0.01$ , the average *P*-value is  $\sim 0.04$ , and 95% of samples have the *P*-value less than 0.12. This analysis shows that there is only 4% probability that the observed sample was drawn from a Gaussian distribution.

The SW test does not have the ability to assess the rather peculiar nature of the *shape* of the observed distribution (i.e., it cannot distinguish the particular nature of non-Gaussianity). To include this information, we consider the small chance (4%) that the measured velocities were drawn from a Gaussian distribution, and estimate the probability that it would produce the observed distribution seen in Figure 5. We generate 10,000 samples and for each sample draw 12 velocities from a Gaussian centered on  $7 \text{ km s}^{-1}$  and  $56 \text{ km s}^{-1}$  wide. Each sample is then divided into velocities greater and smaller than  $7 \text{ km s}^{-1}$ , and dispersions are calculated for each group ( $\sigma^{pos}$  and  $\sigma^{neg}$ ). In only  $\sim 3\%$  of generated samples, the positive velocities have  $7 < \sigma^{pos} < 13$  and negative velocities have  $14 < \sigma^{neg} < 32$ , where

---

<sup>3</sup> [HREF]<http://www.r-project.org/>



the selected ranges reflect the uncertainties in velocity dispersions measured for the observed sample. Therefore, even if the observed velocities were drawn from a Gaussian distribution, it is unlikely they would create the distribution seen in Figure 5.

In light of these results, we conclude that the hypothesis of normality can be rejected at the  $> 95\%$  confidence level. The next simplest explanation for the observed distribution of velocities is that we are observing two velocity groups, one approaching at  $\langle V_{gsr}^{neg} \rangle = -52 \pm 11$  km s $^{-1}$ , and the other one receding at  $\langle V_{gsr}^{pos} \rangle = 50 \pm 3$  km s $^{-1}$ .

In Figure 1, the stars belonging to two velocity groups are shown in different colors (blue for the positive velocity group and yellow for the negative velocity group). One of the goals of this work was to probe the extension of these groups in space. Our data show that both groups are quite extended in space. The positive velocity group extends from  $349^\circ < R.A. < 357^\circ$ , while the negative velocity group is mostly centered around  $R.A. \sim 355^\circ$  with one star  $10^\circ$  away, at  $R.A. \sim 344^\circ$ . At 83 kpc, these angular extensions correspond to 9 and 15 kpc respectively. The large extensions of these groups are hard to reconcile with bound systems. These groups are therefore most likely remnants of disrupted dwarf galaxies, such as tidal streams, passing through the stripe 82 plane of observation (similarly to the Sagittarius dSph trailing stream, see Figure 12 in Sesar et al. 2010 for an illustration).

In their work, Kollmeier et al. (2009) have observed two velocity groups but did not consider the negative velocity group as a real system due to a small number of stars (only three stars). We have repeated our statistical tests using their sample and original velocities, and have found strong evidence of non-Gaussianity in their distribution of velocities. The average  $P$ -value for their sample is 0.03, and the probability of recreating a distribution of velocities with two peaks from a single Gaussian distribution is less than 0.03%. Therefore, we believe there was ample evidence in Kollmeier et al. (2009) for detection of two velocity groups, even before four new observations from this work are added. However, the real benefit of new observations, and of this work, is the increased angular coverage of the Pisces region. The angular extension of velocity groups is now more evident than in Kollmeier et al. (2009), making the velocity groups more likely to be unbound (tidal streams) than bound (globular clusters or dwarf galaxies).

By combining our and Kollmeier et al. spectroscopic metallicities, we find that the positive velocity group has a median metallicity of  $[Fe/H] = -1.4$  dex and a dispersion of 0.2 dex. The metallicity values for this group range from  $-1.1$  dex to  $-1.6$  dex. The metallicity of star 377927 was not used in this estimate due to low S/N of its observed spectrum. The negative velocity group seems to be more metal-poor, with a median metallicity of  $[Fe/H] = -1.7$  dex, dispersion of 0.3 dex, and with metallicities ranging from  $-1.6$  dex to  $-1.9$  dex. The number of stars in each group is small enough, and the errors are large

enough, that we cannot discard the hypothesis that the metallicities are drawn from the same parent population. However, both groups are metal-poor suggesting that the progenitors of these two substructures are systems with old, metal-poor populations.

#### 4. Conclusions

We confirm the existence of two kinematic groups in the Pisces overdensity, located at 83 kpc from the Sun, by combining new spectroscopic observations with those previously obtained by Kollmeier et al. (2009). The spatial extent of groups in the right ascension direction suggests that these are not bound systems but rather debris of disrupted dwarf galaxies, most likely tidal streams. If these are tidal streams, the question remains whether they have the same or different progenitors. The first case (same progenitor) is not an improbable one. The Sagittarius dSph galaxy has already shown us examples where debris stripped in different epochs overlap in the same region of the sky (see Figure 1 in Law et al. 2005). In such regions large gradients in  $V_{gsr}$  are evident along the same line of sight as some streams recede while others approach. The second case (different progenitors) is supported by state-of-the-art simulations of galaxy formation. These simulations predict numerous substructures of different morphologies (streams, shells, clouds) in halos of Milky Way-size galaxies (Johnston et al. 2008). Such substructures may overlap and may be difficult to separate without wide and deep sky coverage.

Ongoing and upcoming wide-area surveys, such as Pan-STARRS (Kaiser et al. 2002) and LSST (Ivezić et al. 2008b), will provide the depth and sky coverage needed to separate different halo substructures in coordinate space. With single-epoch and co-added observations, these surveys will be able to observe main sequence F dwarfs up to distances of 100 kpc and beyond, and will trace halo substructures with greater fidelity. In addition, detections of overdensities in main sequence and RR Lyrae stars will allow robust measurements of metallicities using a photometric method described in Sesar et al. (2010).

This research was supported in part by the National Science Foundation under Grant No. PHY05-51164. B. S. and Ž. I. acknowledge support by NSF grants AST 61-5991 and AST 07-07901, and by NSF grant AST 05-51161 to LSST for design and development activity. Based on observations obtained at the Gemini Observatory, which is operated by the Association of Universities for Research in Astronomy, Inc., under a cooperative agreement with the NSF on behalf of the Gemini partnership: the National Science Foundation (United States), the Science and Technology Facilities Council (United Kingdom), the National Research Council (Canada), CONICYT (Chile), the Australian Research Council (Australia), Ministério da

Ciência e Tecnologia (Brazil) and Ministerio de Ciencia, Tecnología e Innovación Productiva (Argentina). We are grateful to the support staff at Gemini Observatory for their help during both the Phase II preparation and observations of our program. We thank particularly Rodrigo Carrasco for his valuable suggestions.

## REFERENCES

- Allington-Smith, J. et al. 2002, *PASP*, 114, 892
- Belokurov, V. et al. 2007a, *ApJ*, 657, L89
- Belokurov, V. et al. 2007b, *ApJ*, 658, 337
- Binney, J., & Merrifield, M. 1998, *Galactic astronomy*, ed. Binney, J. & Merrifield, M.
- Brown, W. R. et al. 2010, *AJ*, 139, 59
- Chaboyer, B. 1999, in “Post-Hipparcos cosmic candles”, Eds. A. Heck & F. Caputo, Kluwer Academic Publishers, p. 111
- Clewley, L., & Kinman, T. D. 2006, *MNRAS*, 371, L11
- D’Agostino, R. B. & Stephens, M. A. 1986, *Goodness of Fit Techniques* (New York: Marcel Dekker)
- Duffau, S., Zinn, R., Vivas, A. K., Carraro, G., Méndez, R. A., Winnick, R., & Gallart, C. 2006, *ApJ*, 636, L97
- Gratton, R. G. et al. 2004, *A&A*, 421, 937
- Grillmair, C. J. 2009, *ApJ*, 693, 1118
- Harding, P. et al. 2001, *AJ*, 122, 1397
- Helmi, A. 2008, *A&A Rev.*, 15, 145
- Ibata, R. A. et al. 2002, *MNRAS*, 332, 921
- Ibata, R. A., Irwin, M. J., Lewis, G. F., Ferguson, A. M. N., & Tanvir, N. 2003, *MNRAS*, 340, L21
- Ivezić, Ž. et al. 2000, *AJ*, 120, 963
- Ivezić, Ž. et al., 2008a, *ApJ*, 684, 287

- Ivezić, Ž. et al. 2008b, arXiv:0805.2366
- Johnston, K. V. et al. 2008, ApJ, 689, 936
- Jurić, M. et al. 2008, ApJ, 673, 864
- Kaiser, N. et al. 2002, Proc. SPIE, 4836, 154
- Klypin, A. et al. 1999, ApJ, 522, 82
- Kollmeier, J. A. et al. 2009, ApJ, 705, L158
- Law, D. R., Johnston, K. V., & Majewski, S. R. 2005, ApJ, 619, 807
- Layden, A. C. 1994, AJ, 108, 1016
- Majewski, S. R., Skrutskie, M. F., Weinberg, M. D., & Ostheimer, J. C. 2003, ApJ, 599, 1082
- Mateo, M. L. 1998, ARA&A, 36, 435
- Moultaka, J., Ilovaisky, S. A., Prugniel, P., & Soubiran, C. 2004, PASP, 116, 693
- Newberg, H. J., Yanny, B., Cole, N., Beers, T. C., Re Fiorentin, P., Schneider, D. P., & Wilhelm, R. 2007, ApJ, 668, 221
- Prior, S. L., Da Costa, G. S., Keller, S. C., & Murphy, S. J. 2009, ApJ, 691, 306
- Rocha-Pinto, H. J., Majewski, S. R., Skrutskie, M. F., Crane, J. D., & Patterson, R. J. 2004, ApJ, 615, 732
- Schlegel, D. J., Finkbeiner, D. P., & Davis, M. 1998, ApJ, 500, 525
- Sesar, B. et al. 2007, AJ, 134, 2236
- Sesar, B. et al. 2010, ApJ, 708, 717
- Shapiro, S. S., & Wilk, M. B. 1965, Biometrika, 52, 591
- Starkenburg, E. et al. 2009, ApJ, 698, 567
- Schlaufman, K. C. et al. 2009, ApJ, 703, 2177
- van Dokum, P. G. 2001, PASP, 113, 1420

Vivas, A. K., Jaffé, Y. L., Zinn, R., Winnick, R., Duffau, S., & Mateu, C. 2008, *AJ*, 136, 1645

Vivas, A. K. et al. 2001, *ApJ*, 554, L33

Vivas, A. K., Zinn, R., & Gallart, C. 2005, *AJ*, 129, 189

Watkins, L. L. et al. 2009, *MNRAS*, 398, 1757

Yanny, B. et al. 2000, *ApJ*, 540, 825

Yanny, B. et al. 2003, *ApJ*, 588, 824

York, D. G. et al. 2000, *AJ*, 120, 1579

Table 1. RR Lyrae Targets

ID <sup>a</sup>	R.A. <sup>b</sup> (deg)	Dec <sup>b</sup> (deg)	Period (d)	d <sup>c</sup> (kpc)	HJD <sub>0</sub> <sup>d</sup> (+2450000 d)	HJD <sub>spectrum</sub> <sup>e</sup> (+1450000 d)	Phase <sup>f</sup>	$V_r^g$ (km s <sup>-1</sup> )	$V_\gamma^h$ (km s <sup>-1</sup> )	$\sigma_\gamma^h$ (km s <sup>-1</sup> )	$V_{gsr}^i$ (km s <sup>-1</sup> )	[Fe/H] <sup>j</sup>
343892	352.469872	-1.171239	0.59731	83	3352.59737	5064.64036	0.239	-91	-57	10	58	-1.1
377927	350.637200	-1.045226	0.48092	83	3637.73839	5064.87133	0.514	-53	-55	18	63	-1.7*
490555	349.544995	0.856966	0.63091	83	3666.70100	5065.86722	0.689	-49	-72	18	53	...
719918	344.484556	0.333060	0.62337	84	4388.77431	5064.79280	0.466	-186	-182	16	-51	-1.9
3988771	357.351934	0.759800	0.60580	78	4412.73725	5064.72046	0.226	-69	-36	16	76	-1.7

<sup>a</sup>RR Lyrae ID number from the Sesar et al. (2010) catalog

<sup>b</sup>Equatorial J2000.0 right ascension and declination

<sup>c</sup>Heliocentric/galactocentric distance

<sup>d</sup>Heliocentric Julian Date of maximum brightness

<sup>e</sup>Heliocentric Julian Date when the spectrum was taken

<sup>f</sup>Pulsation phase when the spectrum was taken

<sup>g</sup>Radial velocity (not corrected for pulsations)

<sup>h</sup>Systemic (center-of-mass) velocity (corrected for pulsations) and its uncertainty

<sup>i</sup>Galactocentric rest-frame velocity

<sup>j</sup>Spectroscopic metallicity, \* denotes uncertain values

Table 2. Contributions to the error in  $V_\gamma$

ID	$\sigma_{cc}^a$ (km s <sup>-1</sup> )	$\sigma_{\text{templates}}^b$ (km s <sup>-1</sup> )	$\sigma_r^c$ (km s <sup>-1</sup> )	$\sigma_{\text{model}}^d$ (km s <sup>-1</sup> )
343892	7.4	2.3	9.5	13.5
377927	11.8	3.7	13.2	12.0
490555	11.9	3.2	13.3	12.8
719918	8.9	0.5	10.7	12.0
3988771	6.4	2.9	8.7	13.6

<sup>a</sup>Average cross-correlation error

<sup>b</sup>Standard deviation of  $V_r$  values obtained from cross-correlations

<sup>c</sup>Uncertainty in measured radial velocity

<sup>d</sup>Uncertainty in model radial velocity

Table 3. Revision of velocities from Kollmeier et al. (2009)

ID	R.A.	Dec	Phase	$V_r$ (Observed) (km s <sup>-1</sup> )	$V_\gamma$ (Kollmeier et al.) (km s <sup>-1</sup> )	$V_\gamma$ (This work) (km s <sup>-1</sup> )	Difference (km s <sup>-1</sup> )	$V_{gsr}$ (This work) (km s <sup>-1</sup> )
	(deg)	(deg)						
343892	352.469872	-1.171239	0.422	-63	-68	-57	11	58
3115111	354.116700	-0.384237	0.362	-156	-156	-140	16	-26
349151	354.878980	-0.157729	0.436	-192	-198	-184	14	-71
359035	354.955497	-0.276307	0.335	-192	-189	-172	17	-59
3981578	355.577586	-0.008393	0.388	-82	-84	-69	15	44
3974293	355.600850	-0.623494	0.404	-84	-87	-72	15	39
3944324	355.750750	-0.173178	0.425	-65	-70	-56	14	56
3879827	356.294558	-0.804956	0.315	-73	-68	-51	17	58



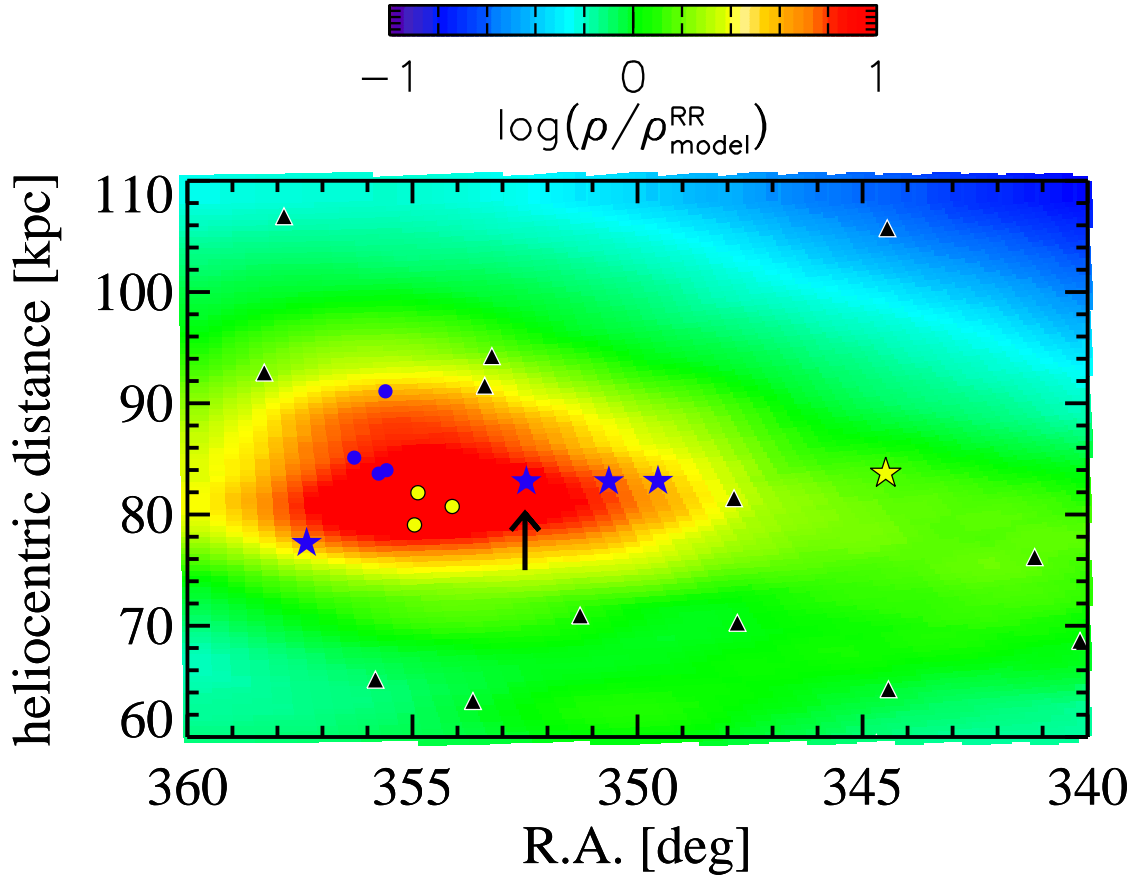


Fig. 1.— A zoom-in of Fig. 11 from Sesar et al. (2010) showing the spatial distribution of RRab stars located in the vicinity of the Pisces overdensity (red and yellow region). Due to their angular position, the heliocentric and galactocentric distances of these stars are virtually the same. The colored background shows the observed number density of RR Lyrae stars ( $\rho$ ) relative to expected smooth model number density ( $\rho_{model}^{RR}$ , Eq. 16 in Sesar et al. 2010). The observed number density in the red region is 10 times greater than the model prediction. The RRab stars were selected from the Sesar et al. (2010) stripe 82 catalog and have  $|Dec| < 1.25^\circ$ . The stars spectroscopically observed by Kollmeier et al. (2009) are shown as solid circles, those observed in this work are shown as starred symbols, and stars not yet spectroscopically observed are shown as triangles. The arrow points to a star that was observed in this work and by Kollmeier et al. (2009). The blue and yellow symbols show stars associated with  $\langle V_{gsr} \rangle = 50 \text{ km s}^{-1}$  and  $\langle V_{gsr} \rangle = -52 \text{ km s}^{-1}$  velocity groups, respectively. The positions, velocities, and metallicities of spectroscopically observed stars are listed in Table 1.

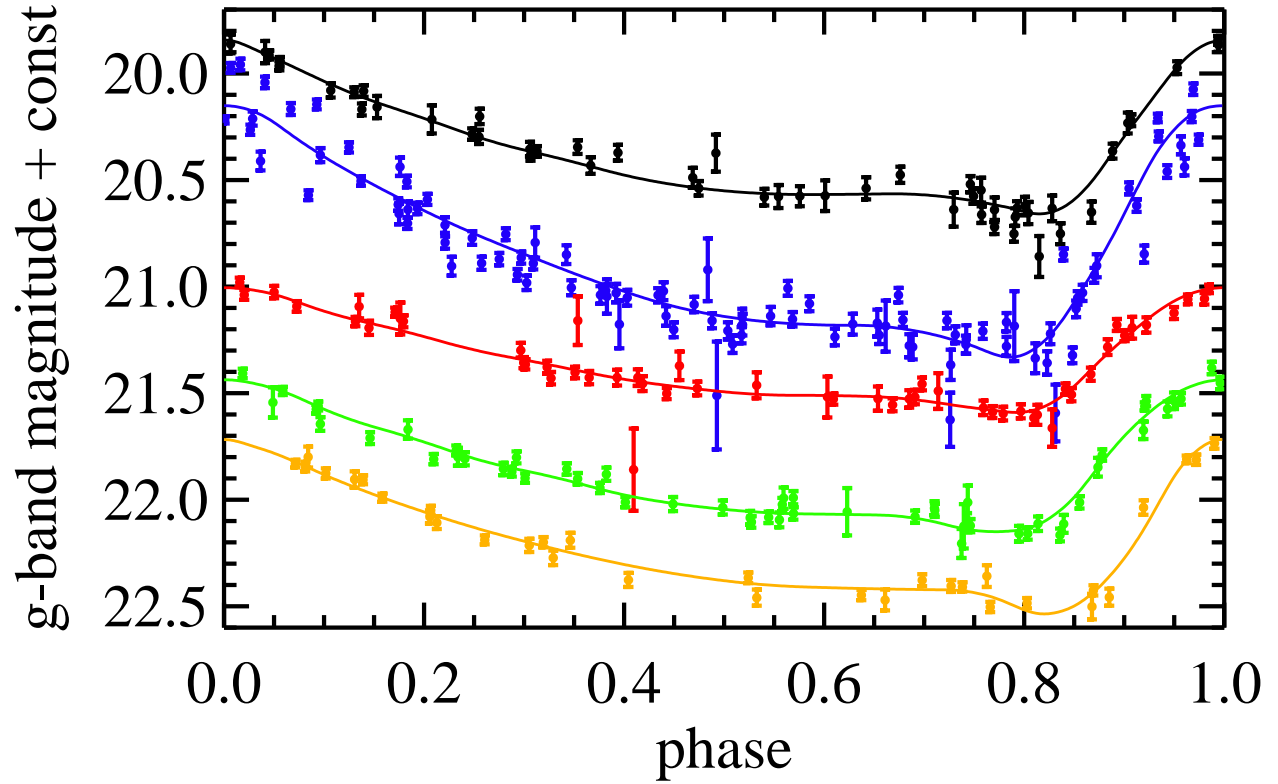


Fig. 2.— The  $g$ -band light curves of observed stripe 82 RR Lyrae stars, ordered as in Table 1. The magnitudes are corrected for the ISM extinction using the map from Schlegel et al. (1998). The light curves are offset for clarity. The solid lines show best-fit  $g$ -band templates from Sesar et al. (2010).

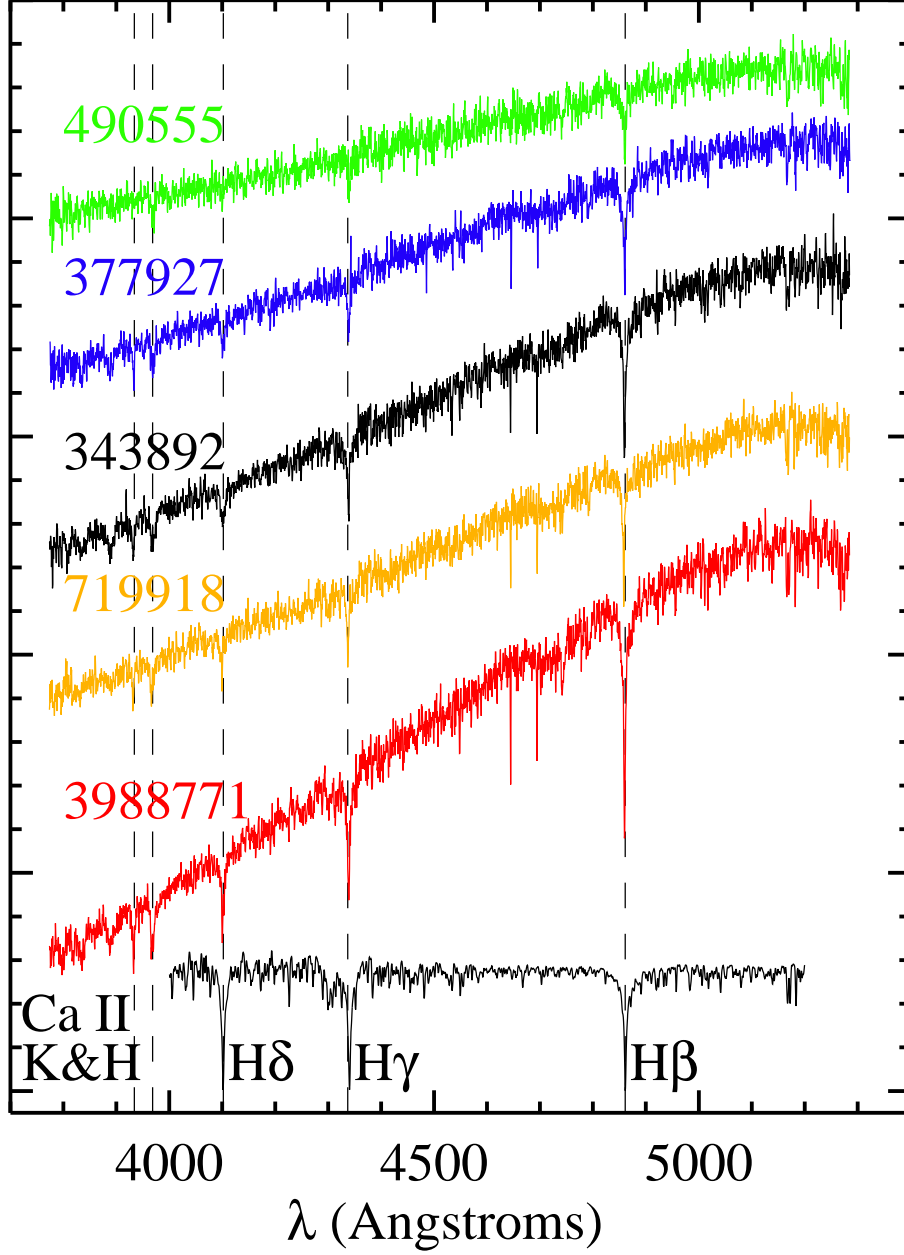


Fig. 3.— GMOS-S spectra of the 5 RR Lyrae stars observed in the Pisces overdensity, ordered from lowest to highest S/N (top to bottom). An ELODIE template spectrum (normalized to continuum) is shown at the bottom of the panel. The dashed lines show the positions of important spectral features.

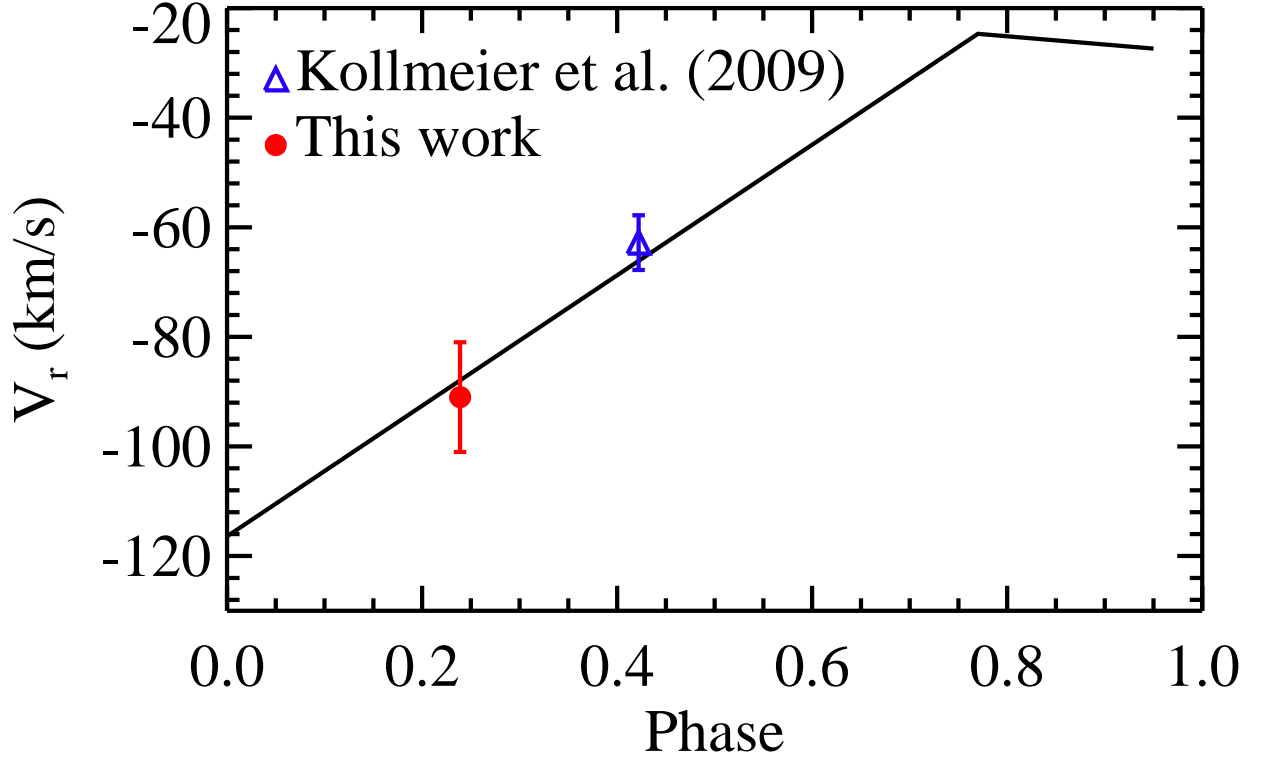


Fig. 4.— Radial velocity observations of star 343892 (indicated by an arrow in Fig. 1). The solid line is the template of the radial velocity curve of RRab star X Arietis shifted in velocity to fit the observations.

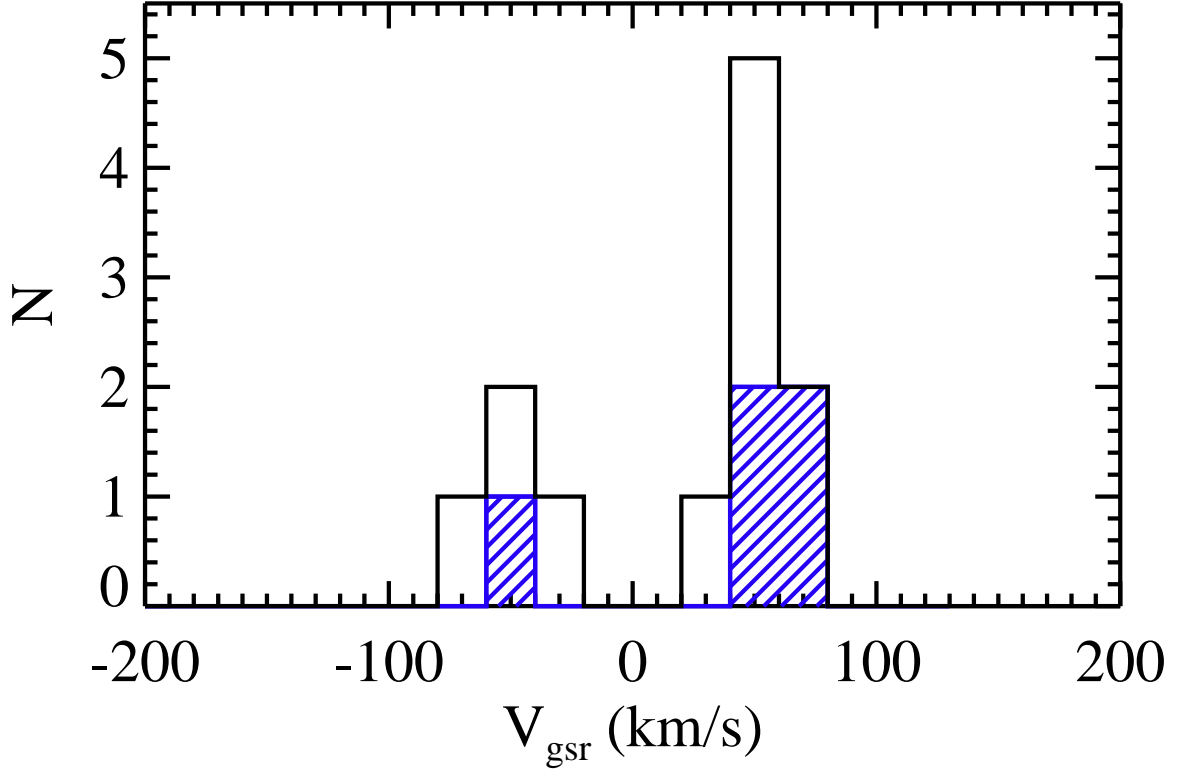


Fig. 5.— Histogram of  $V_{gsr}$  of the combined sample of RR Lyrae stars in the Pisces overdensity. The shaded histogram includes only stars observed in this work. The bin size is  $20 \text{ km s}^{-1}$ , and is slightly larger than the largest radial velocity error ( $18 \text{ km s}^{-1}$ ). The distribution of observed velocities seems to be bimodal, with two velocity peaks centered on  $\langle V_{gsr} \rangle = -52 \text{ km s}^{-1}$  and  $\langle V_{gsr} \rangle = 50 \text{ km s}^{-1}$ , respectively. See the text for a discussion of statistical significance of this bimodality.